Experimental Mechanics (2014) 54:1215–1226
DOI 10.1007/s11340-014-9894-y

Micro-Scale Restraint Methodology for Humidity Induced Swelling Investigated by Phase Contrast X-Ray Tomography

A. Patera · K. Jefimovs · A. Rafsanjani · F. Voisard · R. Mokso · D. Derome · J. Carmeliet

Received: 18 May 2013 / Accepted: 14 April 2014 / Published online: 7 May 2014

Abstract A new methodology for restraining the swelling of spruce wood samples in the micrometre range is developed and presented. We show that the restraining device successfully prevents the free swelling of wood during moisture adsorption, thus modifying significantly the anisotropy of swelling and provoking the intended collapse and large deformations of the wood cells at the edges of the sample in contact with the restraining device. The device consists in a slotted cube designed to restrain swelling and is made of PMMA manufactured by laser ablation. The sample undergoing the restraining experiment is imaged with high-resolution synchrotron radiation phase contrast X-Ray Tomographic Microscopy. The deformation of the restraining device itself is only approximately 2 μm with respect to a 500 μm width in cubes containing latewood samples and half of that in the case of cubes containing earlywood.

A. Patera (✉) · A. Rafsanjani · D. Derome · J. Carmeliet
Laboratory of Building Science and Technology, EMPA, Swiss Federal Laboratories for Materials Science and Technology, Dübendorf, Switzerland
e-mail: alessandra.patera@empa.ch

K. Jefimovs
Laboratory for Electronics/Metrology/Reliability, EMPA, Swiss Federal Laboratories for Material Science and Technology, Dübendorf, Switzerland

F. Voisard
Department of Mining and Materials Engineering, McGill University Montreal, Montréal, QC, Canada

A. Patera · J. Carmeliet
Chair of Building Physics, ETH Zürich, Zürich, Switzerland

R. Mokso
Paul Scherrer Institut, Villigen, Switzerland

Keywords Spruce wood · Microscopic swelling · Phase Contrast · Synchrotron X-ray Tomography · Moisture sorption · Plexiglas · Restraining device

Introduction

Wood is a natural material known to swell and shrink when exposed to various levels of relative humidity (RH). A main feature of wood, especially when growing in temperate climate, is its yearly growth ring, where thin-walled large cells of the earlywood grow in spring and thick-walled smaller cells of latewood grow in summer. The cell wall material is composed of a natural composite of crystalline cellulose fibers immersed in a hydrophilic polymeric matrix of amorphous cellulose, hemicelluloses and lignin. Given the low absorption of X-ray by wood, phase contrast X-ray microscopy is a technique well-suited for the study of free hygroscopic swelling of wood at cellular scale, as reported in our previous works [1, 2]. The free swelling/shrinkage of wood was investigated at cellular scale, leading to the conclusion that, in addition to a general global swelling, local deformations occur within the cellular structure. These deformations should be even more significant when the swelling of the wood cells is subjected to an external restraint during hygroscopic cycles. It is long known that internal strains influence the radial and the tangential swelling rate of wood sample [3]. In [4], the swelling pressure during swelling of red oak was measured with electrical resistance strain-gage load cells designed to prevent the swelling. The swelling pressure was higher in tangential than in radial direction from dry to 50%RH, while similar in the two directions from 50 to 80 %RH. Although the mechanism of restraining swelling of wood during moisture sorption has been of interest, most of these investigations are performed at the macroscale (e.g., [5–7]). Documenting restrained swelling at the microscale could lead to a better understanding of

the differential swelling undergoing in large timber exposed to varying environmental conditions, thus to gradient in moisture content. Such differential swelling is known to lead to wood checks and cracking over long time.

In this paper, we present a novel and efficient technique to verify the occurrence of local deformations at cellular scale, by restraining a microscopic piece of wood undergoing swelling. Polymethylmethacrylate (PMMA or plexiglas) cubes were used to restrain the free swelling of wood samples subjected to relative humidity changes. The fabrication of the restraining device is performed in two steps, where first an industrial laser machine is used to produce the initial cubic structure and, subsequently, the cube slot housing the wood sample is cut with high-precision ps-laser ablation. The main challenges are the selection of the material for the restraining device which should be machinable with high-precision, transparent to X-rays, and provide sufficient stiffness and the attainment of perfect contact of the surfaces receiving the sample. This paper relates the design of the device, its fabrication combining mechanical and laser ablation processes and its use during an experiment using synchrotron X-ray phase contrast microtomography. The experiments highlight the capacity of the manufactured device to restrain swelling of wood and induce local deformation on the wood cells. We perform two- and three-dimensional analyses in order to identify the restraint effect of the device.

Design of the Restraining Device: Material and Method

We present in this section the different steps taken towards designing the restraining device.

Restraining Method

In recent years, micromechanical setups devised for tomography have been developed in order to study the microstructure of various materials under mechanical loading. For example, [8] developed a micro-compression device for bone testing to assess the dynamic image-guided failure of bone ultrastructure and bone micro-damage and [9] made a compression testing device to determine the cellular response of wood under mechanical loading. These devices are made of three main components: (a) a linear stepper motor which is attached to the micro load-cell; (b) a sample stage and (c) an outer cylinder made of carbon fibre reinforced plastic to transmit the load without absorbing X-ray, the whole set-up being able to rotate. In both cases, the samples can be subjected to compression until mechanical failure. However, neither system can be used to expose the samples to varying RH conditions, due to the limitations in their designs. As few devices for micro-compression test set-ups are suitable for X-ray microtomography experiments under controlled RH and temperature conditions, an innovative method is sought to restrain micrometre-sized wood samples subjected to hygroscopic loading.

The aim is to design a restraining device which fits within an environmental chamber with controlled air conditions. Therefore, we considered a passive mode of restraint during swelling by producing a device that resists the swelling of the sample. A first complexity is posed by the natural cellular structure of wood, which makes it impossible to produce a plane surface as cutting through cells results always in dented surfaces. We resorted to fabricate a solid restraining device that would restrict swelling in one direction. Another design constraint was that both the wood sample and its contact with the restraining device must fit within the field of view (FOV) of the microscopic setup to reach high-resolution. So the chosen approach was to insert the sample within a slotted cubic device. The slot should provide two flat smooth surfaces to restrain the displacement of the sample undergoing swelling and should be visible in the FOV. In addition, the slot allows humid air to access the sample.

Selection of the Material of the Restraining Device

The main features required for the material in the fabrication of the restraining device are high stiffness and transparency to X-rays. The need for X-ray transparency disqualifies stiff materials such as ceramics and metals. Polymers are classified as moderate stiff materials, in a range similar to wood, with a Young's modulus between 0.1 and 10 GPa. Also, given their lower density, polymers are quite transparent to X-rays. A readily available and known polymer is PMMA.

In terms of physical properties, PMMA is a plastic product with excellent optical clarity, good weathering resistance, high tensile strength (48–76 MPa) and tensile modulus. This material is a quite stiff material with a Young's modulus ranging between 1.8 and 3.1 GPa. Young's modulus of polymers varies with environmental factors such as temperature and humidity. PMMA is reported to absorb water with a maximum of water absorption ratio of 0.3–0.4 % by weight. Swelling of PMMA by water sorption is equal to 0.4 % at 25 °C and 100 % RH [10]. PMMA Young's modulus decreases linearly with increasing RH [11–13].

The chemical formula of PMMA is $(C_5O_2H_8)_n$ with density ρ=1,190 kg/m^3. In [14], the mass attenuation coefficient of polymer compounds is calculated at photon energies from 1 keV to 20 MeV with:

$$\mu/\rho = \sum\nolimits_{\mathrm{i}} w_{\mathrm{i}} (\mu/\rho)_{\mathrm{i}} \tag{1}$$

where w_i is the fraction by weight of the ith atomic constituent and $(\mu/\rho)_i$ is the mass attenuation coefficient of each constituent element. This results in a mass attenuation coefficient of

$\mu/\rho=0.5714 cm^2/g$ in PMMA for $E=20$ keV, meaning that this material is relatively transparent to X-rays [15].

The transparency of PMMA is required to allow the X-ray to pass through the restraining device and to interact mainly with the wood sample. A 20 keV photon energy, which is the energy level used at the TOMCAT beamline of Swiss Light Source (SLS) during the current experiments, is reported not to produce damage to the PMMA [16].

Thus, for its transparency to X-ray and its high stiffness, PMMA satisfies the requirements for the restraing device.

Dimensioning of the Restraining Device

In order to restrain the swelling of the wood sample, the dimensions of the cube and the slots are optimized to provide an appropriate rigidity of the device and optimum space for image acquisition. For this purpose, a finite element parametric study is carried out to estimate the deformation of the device and slot boundaries under swelling pressures. The swelling pressure of the spruce wood from dry to high RH is known to be about 2 MPA, based on macroscopic experiments (e.g. [17]). The selected material, PMMA, is elastic isotropically with elastic Young's modulus $E=3$ GPa and Poisson's ratio $\upsilon=0.3$. Different geometries are considered. The effect of swelling load is applied as a uniform pressure on the top and bottom surfaces of the slot in a region of 1 mm width through the whole opening and the deformation of the cube is calculated using the finite element package ABAQUS (Rising Sun Mills, USA). The results of the simulations for different combinations of the cube and slot sizes in terms of the deformation in the Y-direction are shown in Fig. 1. The $2\times2\times2$ mm^3 cube is subjected to higher deformations compared with the two bigger cubes under the above mentioned conditions. Smaller deformations occur in the $3\times3\times3$ mm^3 PMMA cube under load, while intermediate values are found in the $4\times4\times4$ mm^3 device. Based on this study, the $3\times3\times3$ mm^3 and the $4\times4\times4$ mm^3 cubes are selected as providing good restraint to the swelling of the wood samples.

Production of the Restraining Device

In a first trial, a PMMA cube of $4\times4\times4$ mm^3 with a slot of 1 mm height and 2 mm width was produced with an industrial laser cutting machine. The defects on the slot produced during its manufacture resulted in discontinuous contact areas with the wood sample due to melting of PMMA, which was detected by the tomographic images. To avoid such difficulties, an improved restraining device is manufactured by combining picosecond laser ablation and mechanical processing, enabling the drilling of a flat, precise and smaller slot in the cube, thus allowing a use of smaller samples and therefore achieving a higher image resolution.

Micromachining by ps-laser Ablation

The picosecond (ps)-laser ablation system is used to produce the device. Such laser system has many applications in micromachining, such as micro-structuring surfaces, micro-cutting and micro-drilling thin materials up to a few millimetres thick. The ps-laser can ablate any type of material (polymers, metals, semiconductors, glasses, and ceramics) without mechanical force, without wear and tear and without thermal damages. The YAG (yttrium aluminium garnet)-laser operates at 1,064, 532 and 355 nm with repetition rates 0–500 kHz and average power up to 10 W at 1,064 nm and up to 4 W at 355 nm. The scanning of the beam over the sample is possible either by precise XY stages with travel range 350×210 mm^2 or with galvanic scanner covering 50×50 mm^2 area. The sample is positioned in the path of the beam by a CCD camera with accuracy better than 10 μm.

The material removal rate as a function of average power at 50 kHz frequency is calibrated on a 2 mm thick PMMA sample. The resulting depth and roughness are measured with the Tencor P-10 Surface Profiler. A stylus scans the sample across the grooves produced by the laser, which are schematically shown in Fig. 2(a). The depth as a function of the power is plotted in Fig. 2(b). As can be seen from Fig. 2(b), the material is not removed at power level of 50 mW, which appears to be below the ablation threshold for the parameters used. On the other hand, we also see a strong increase of the removal rate at the power level of 1 W. We have noted that material melting takes place at this power level, which makes the ablation process similar to that of ns-laser. The dependence of the removal rate on power was found to be quite linear in a 150–700 mW range. We have chosen 500 mW to produce the $0.5\times2\times4$ mm^3 (depth, width and length) slot in the $4\times4\times4$ mm^3 cubes (see Fig. 2) and the $0.5\times1\times3$ mm^3 slot on the $3\times3\times3$ mm^3 samples.

Fabrication of the Restraining Device

We found that the mechanical production of the cubes and slots with the required dimensions appeared to be difficult, since fabrication by ns-laser leads to local melting of the PMMA, while fabrication by ps-laser is relatively slow and leads to tapered sidewalls. Thus we used the advantages of laser ablation and mechanical machining and combined these methods for appropriate fabrication steps. Cubic-shape PMMA samples with dimensions $4\times4\times4$ mm^3 and $3\times3\times3$ mm^3 were first produced by an industrial ns-laser ablation system. The $2\times2\times2$ mm^3 cubes and the slots in the cubes of three sizes were cut by ps-laser ablation using wavelength of 355 nm, frequency of 50 kHz, and a hatch and spot-to spot distance of 3 μm.

The 2 mm-thick devices required a scanning time up to 5 s at 300 mW power at each scan (in the X-Y plane), while the

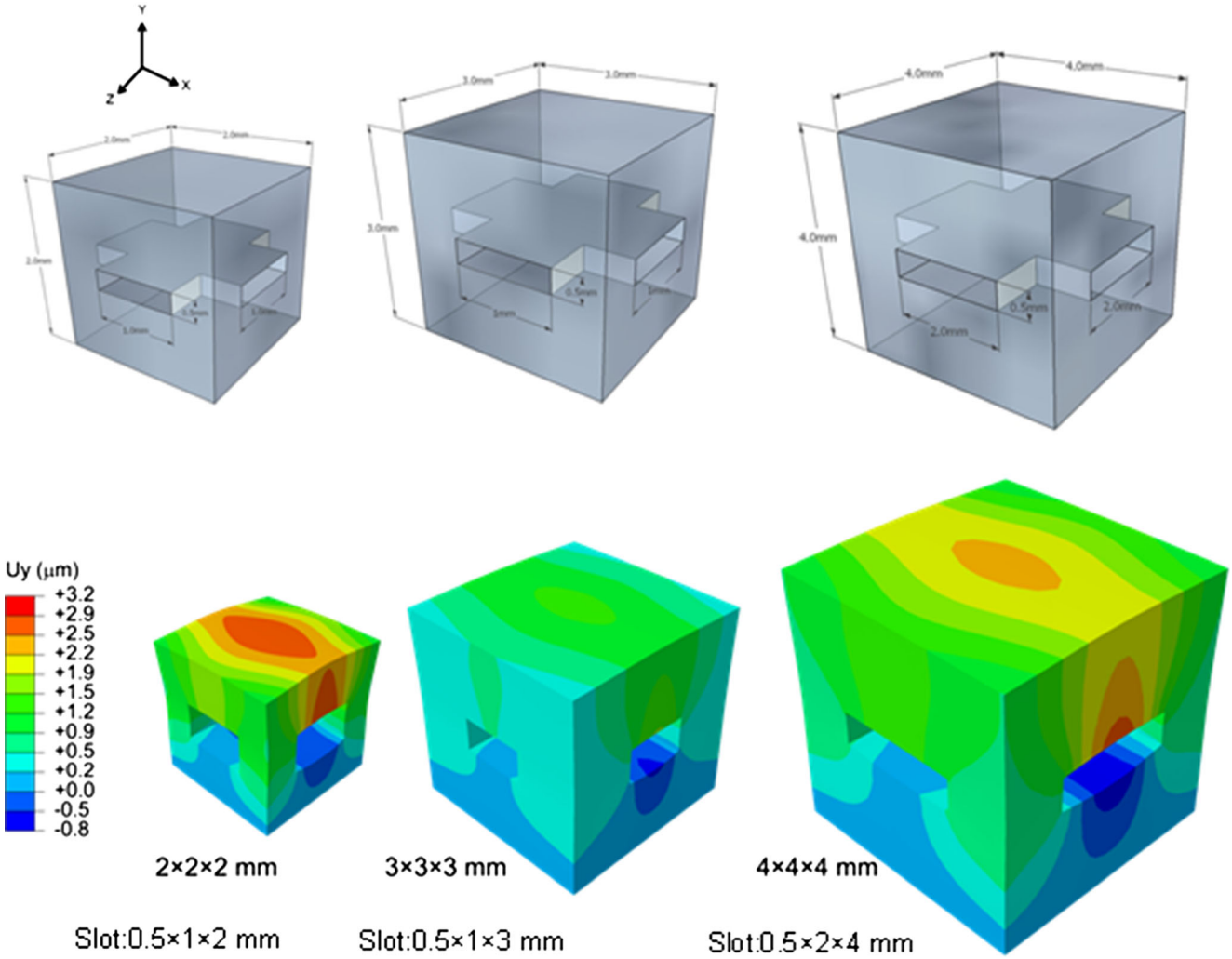

Fig. 1 Above, three-dimensional illustrations of the PMMA cubic sample with the cross-shaped slots, below, displacement field along the y-direction of three different configurations of restraining device

thicker samples needed 10 s for one X-Y scan at higher power (up to 500 mW). The ps-laser ablation allowed manufacturing of even smaller PMMA cubic samples, with a size of 2×2×2 mm^3 and a slot size of 0.5×1×2 mm^3. In this case, the power was decreased down to 300 mW to reduce the melting effects, which were arising on the sample surface during multiple scanning. In total, 10 restraining devices were manufactured.

The procedure followed for the slots preparation is described below:

– The laser beam is scanned in the X-Y directions on one side of the cube to form the first part of the slot. This step leads to the half part of the first slot with a conical shape.

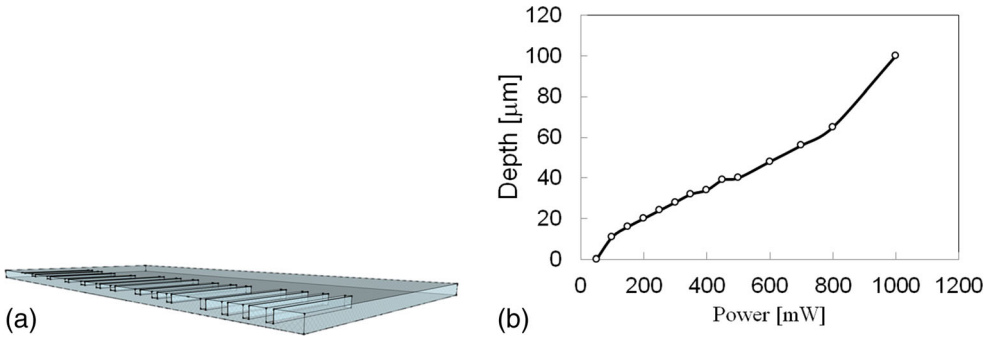

Fig. 2 (**a**) Schematic representation of micro-machining by laser ablation at different power values (from 50 mW to 1 W). (**b**) Graph of depth of groove with one pass in X and Y directions attained versus power used

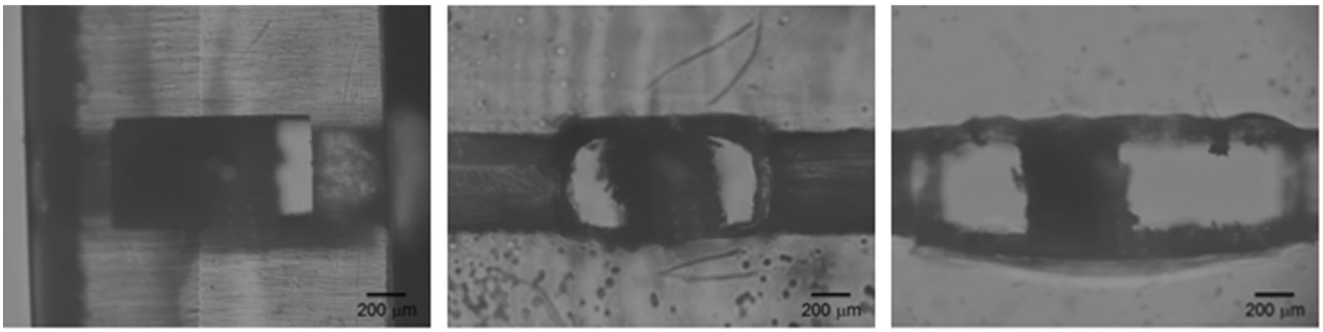

Fig. 3 2D pictures of three wood samples located respectively in (**a**) 2×2×2 mm^3, (**b**) 3×3×3 mm^3, showing cracks and surface roughness, and in (**c**) 4×4×4 mm^3 PMMA cubes, acquired by optical microscopy

- The sample is rotated to the other side (at 180°) to continue the machining of the remaining part of the first slot.
- The first two steps are repeated for the manufacture of the second slot, perpendicular to the first one.
- A 0.5 mm screw (corresponding to the slot depth) is carefully used to remove some remaining material in order to get a rectangular shape for the slot. The manipulation was controlled under an optical microscope.
- Finally, a silicon carbine paper is used to polish the internal slot.

Preparation of the Wood Samples

The 0.5 mm×0.5 mm (tangential and radial cross-sectional dimensions) spruce wood samples (*Picea Abies*, L. Karst) are cut from 20 mm×20 mm×20 mm (tangential, radial and longitudinal directions) wood cubes with a razor blade. As required for the surface of the PMMA slot, the surfaces of the wood samples have also to be as flat and smooth as possible, in order to fit in the slot and to be perfectly in contact with its surface. Laser ablation is not appropriate for the wood samples preparation, since it leads to burning and internal modification on the wood surface. Thus, wood samples were mounted on the translational stage and cut by razor blade in 0.5 mm slices along the tangential/radial cross-section.

Finally, the samples are manually cut along the longitudinal direction with the proper length (corresponding to half of the slot length) with a razor blade. Then, the samples are placed in a dry desiccator until placement in the restraining devices.

Table 1 Initial dimensions of the wood samples before insertion into the cubes

Samples/Loading direction	Latewood	Earlywood
Tangential	690 μm	520 μm
Radial	600 μm	460 μm

Mounting of the Samples

The dimensions of the wood samples are 0.5 mm×0.5 mm×1 mm (tangential×radial×longitudinal directions) to be inserted in a 2×2×2 mm^3 restraining device, 0.5 mm×0.5 mm×1.5 mm for the 3×3×3 mm^3 device, and 0.5 mm×0.5 mm×2 mm for the 4×4×4 mm^3 device. Once inserted, the samples are observed under an optical microscope in order to observe and quantify the size of the wood samples, the smoothness of the slot surfaces and the quality of contact between wood samples and slots as shown in Fig. 3.

The wood samples for the PMMA cubes are first kept in a desiccator over desiccant for 3 days to reach dry state. Then, one series of the mounted samples are placed in the desiccator with water to reach the 100 % RH equilibrium for 3 days and again visualized under the optical microscope. A visual comparison between the two states allows to conclude that the 4×4×4 mm^3 PMMA cubes exert a major constraint to the free swelling of wood compared to the two smaller systems. Further observations highlight roughness on the slot surface and presence of cracks and bubbles in the 3×3×3 mm^3 cubes (see Fig. 3(b)). Using the images, the position of the wood samples

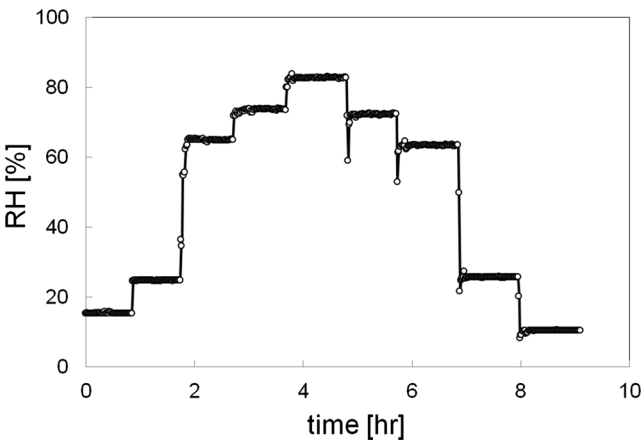

Fig. 4 Typical hygroscopic loading protocol representing the different RH values to which wood samples are exposed during the tomographic scans

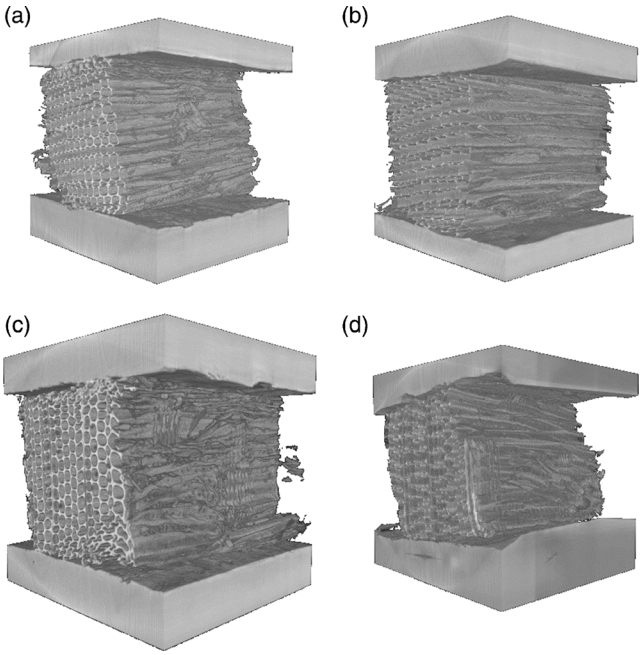

Fig. 5 Volume rendering on four datasets at 10 %RH for (**a**) latewood in tangential direction, (**b**) earlywood in tangential direction, (**c**) latewood in radial direction and (**d**) earlywood in radial direction

in the cubes is optimized under the optical microscope and their tangential and radial dimensions are measured and reported in Table 1.

Experimental Procedure: Setup and Tomography

The measurements are carried out at the TOMCAT beamline of Swiss Light Source (SLS), Paul Scherrer Institut. The experimental setup consists of a synchrotron radiation X-Ray Tomographic Microscope for image acquisition and a climatic chamber for conditioning the samples. The wood sample, prepared and located inside the restraining device, is mounted on a rotational stage and scanned with an energy of 20 keV and an exposure time of 40 ms. The detector to sample distance is optimized to 20 mm. A total of 1,000 projections per tomographic scan are acquired with a standard CCD camera, PCO 2000, by employing a 2× binning factor, which results in a field of view (FOV) of 757×757 μm^2 and an effective pixel size of 0.74×74 μm^2. This brings to a 1,024×1,024 pixel effective resolution. Thus, the sample is exposed to only 40 s of X-ray radiation during one scan, a main advantage of using synchrotron radiation X-ray tomography instead of conventional CT towards ensuring that the sample is not damaged, nor deformed by X-rays.

The reconstruction is performed in two steps. First the phase shift introduced by the wood is retrieved using the algorithm based on the homogenous object assumption [18]. This algorithm is derived from the 'transport-of-intensity equation' and is well applicable for the wood samples which are representing a homogenous object for X-rays meaning that its 3D complex refractive distribution consists of only two components: wood and air. Under the approximation of a "homogeneous" object the real and the imaginary parts of the refractive index representing the phase shift and attenuation are proportional to each other and can be calculated from the images acquired at a single propagation distance. After the phase retrieval step we used the Fourier based tomographic reconstruction method [19] to obtain the 3D volumes.

Four wood samples, two of latewood (LW_t and LW_r) and two of earlywood (EW_t and EW_r), are located inside the 4×4×4 mm^3 PMMA cubes. The samples are exposed to relative humidity cycles from RH=15 % to RH=85 % in adsorption and desorption during the tomographic scans. Specifically, the procedures are as follows: LW_t: 15 – 25 – 65 – 75 – 85 – 75 – 65 – 25 – 15 % RH, see results from a RH sensor located inside the environmental chamber in Fig. 4; LW_r: 15 – 65 – 85 – 65 – 2 % RH; EW_t: 15 – 25 – 65 – 75 – 85 – 75 – 65 – 25 – 15 % RH; EW_r: Dry – Wet – Dry. Each RH condition is maintained approximately for one hour before the tomographic scans in order to ensure moisture content equilibrium.

The PMMA cubes and the slots were recognized by identifying their edges and by contact zones between plexiglass and wood. A three dimensional visualization of the four systems is represented in Fig. 5. Volume rendering is performed on the reconstructed datasets for the four samples at dried state.

The system in Fig. 5(d) (radial earlywood) shows a rougher slot surface although the contact with the wood sample is still good. Further, the wood samples squeezed inside the PMMA cubes reveal deformations of some cells at the edges, in particular in the two latewood specimens (Fig. 5(a) and (c)).

Table 2 Maximum increase of the height of the cube slot under the swelling pressure of the four samples

PMMA samples/loading direction	Latewood		Earlywood	
	Absolute	Percentage	Absolute	Percentage
Tangential	2.36 μm	0.5 %	0.79 μm	0.2 %
Radial	1.52 μm	0.3 %	0.22 μm	0.04 %

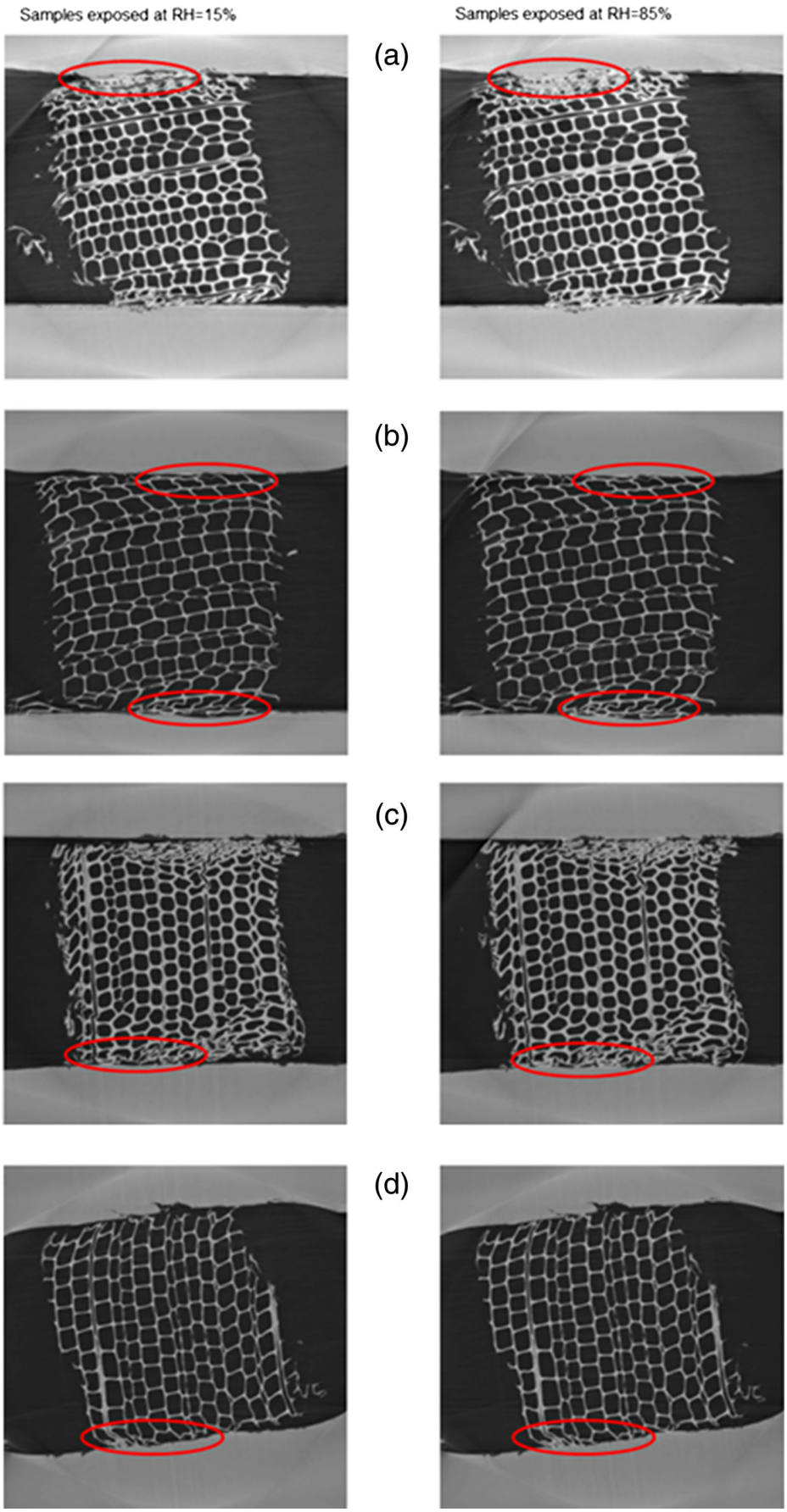

Fig. 6 2D cross-sectional view of wood samples inside the PMMA cubes. (**a**) Latewood in tangential, (**b**) earlywood in tangential, (**c**) latewood in radial, (**d**) earlywood in radial directions (note the different RH values)

Results and Discussion

In this section, the adequacy of the PMMA as a restraining device for wood is demonstrated by 2D image analysis first and then in 3D, with more sophisticated tools.

Two-dimensional Image Analysis Combined with Sorption Analysis of the Cube Slot Surfaces

Two datasets acquired at 15 and 85 % RH for each sample, are compared slice by slice. The main technique adopted for this investigation is affine registration, using the image analysis and visualization toolbox available in Matlab. Affine registration consists in aligning two images by removing the global geometrical differences due to translation, rotation, shear and scaling. The initial four control points given as input to the algorithm are selected across the boundary of the PMMA slot in order to quantify possible deformations of the cube after moisture sorption. The images are pre-processed in order to remove the region of interest (ROI) containing the wood sample and to verify the presence of deformations. Then, the affine registration is performed on the PMMA slots by comparison of two cross-sectional pictures at the same plane and at two RH conditions, i.e. 15 and 85 %. The results are reported in Table 2.

It has been recently documented that, in free swelling, the latewood deforms much more isotropically than earlywood which is markedly anisotropy, and that the ratios of tangential to radial swelling is increasing with decreasing porosity [2].

Four different samples were squeezed inside the PMMA slots provoking an initial collapse of some cells at the edges of the sample and, consequently, an initial expansion of the slot near the contact regions (as showed in the scans at 15 % RH). The scans at 85 % RH show that the cell collapse is clearly increasing during the swelling of the cell wall due to water sorption, as highlighted by red circles in Fig. 6.

The wood sample exerts a pressure on the PMMA, due to the swelling pressure in spruce wood samples. We predicted by simulations that the maximum strain along the Y direction under the conditions of a cube of size $4\times4\times4$ mm^3 with slot cross section of 0.5×2 mm^2 would be equal to 2.8 μm. The maximum deformation, resulting from the experiments for RH=85 %, ranges between 0.22 and 2.36 μm. This result shows the adequacy of the design methodology for optimizing the geometry of the restraining device for the experiments.

In addition, we performed a dynamic vapour sorption (DVS) measurement on a PMMA cube, in order to verify the hygroscopic behaviour of the restraining device. In Fig. 7, the PMMA moisture content (MC) is plotted versus RH. The MC ranges between 0 and 0.3 % for RH values between 5 % (considered as dry state) and 90 %. Thus, the amount of moisture adsorbed by PMMA in the hygroscopic range is negligible compared with the MC of wood in the same range. This leads to the very small deformations induced by moisture in PMMA.

As shown in Table 2, the deformation of the cube slots due to the swelling of wood from 15 to 85 % RH is equal, in percentage, to 0.5 % in the cube containing the LW_t, 0.3 % in the cube with LW_r, 0.2 and 0.04 % in cubes containing EW_t and EW_t, respectively. Given the swelling of PMMA measured above, then we can say that only the first 0.6–0.8 μm of the slot deformation is due to PMMA swelling and the rest to mechanical deformation due to the stress imposed by the samples.

Also, we see that as the wood samples undergo sorption of water, the cells at edge of the sample and in contact with the restraining surface undergo buckling. Similar mechanism occurs in both tissues but less in latewood. We remind that the samples were cut with a razor blade, thus most likely initially in some deformed or disturbed state due to cutting and insertion into the cube. Such state must facilitate the occurrence of buckling. Although a more detailed analysis of buckling would require local deformation, or non-affine registration, and is not in the scope of the present study, the capacity of the restraining device to lead to buckling is seen.

Three-dimensional Image Analysis on Different ROIs

The four datasets are analysed with 3D image analysis tools in order to determine the level of swelling/shrinkage in the tangential, radial and longitudinal directions of wood. As confirmed from our previous studies [1, 2, 20], the longitudinal strains measured here tend to zero and so are not presented further during this analysis.

Samples LW_t and EW_t show a good contact with the PMMA slot surface during the whole hygroscopic protocol in adsorption and in desorption, except in two RH conditions in desorption at 15 and 25 %. Sample LW_r shows more contact at 85 % RH and then a lower level of contact in the other RH

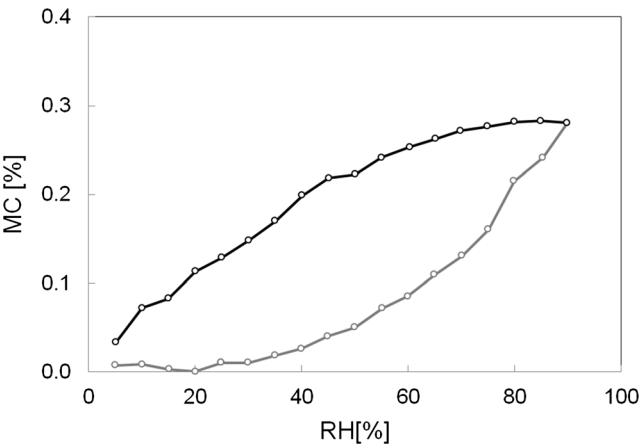

Fig. 7 Dynamic vapour sorption analysis on a PMMA sample. The adsorption and desorption curves are represented respectively in *grey* and *black*

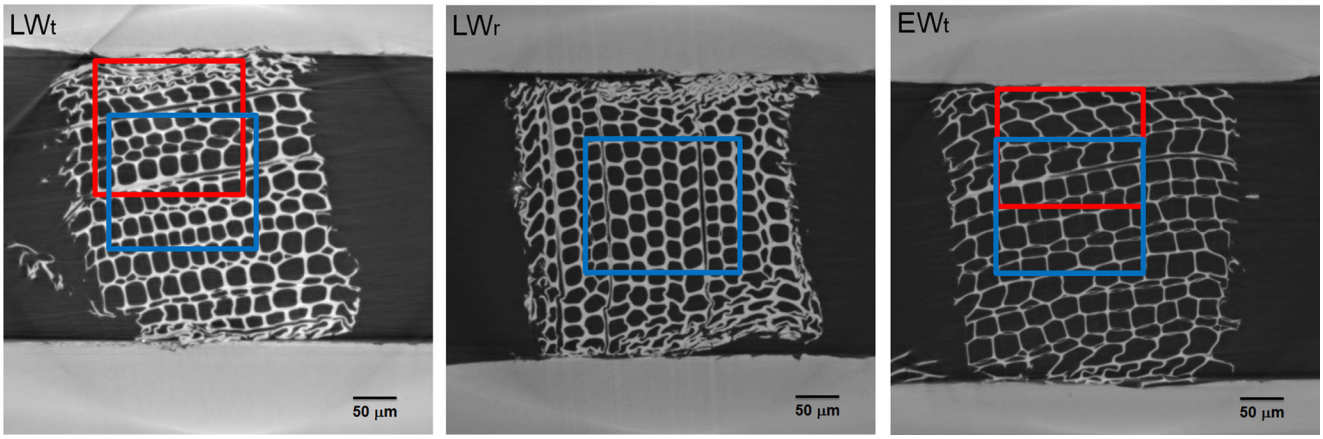

Fig. 8 ROIs considered for this analysis. ROI 1 in *blue* and ROI 2 in *red*

values. Due to setting problems of the environmental control system machine during the tomographic scan, we are unable to recover the exact RH values to which sample EW_r was exposed and, additionally, we notice no contact for this sample to the restraining device, thus we omit this dataset for the 3D analysis.

We consider regions of interest (ROIs) in the centre of the wood samples and at the edges in contact with the PMMA cube, containing from 29 up to 60 cells (see Fig. 8) and we calculate the porosity, the cell wall thickness and the swelling/shrinkage strains in the tangential and radial directions.

The porosity and the cell wall thickness are measured by using the software for image analysis and visualization VG Studio MAX 2.0, while the affine registration for the calculation of the strains is performed with 3D Slicer [21].

The cellular porosity is defined as the ratio of the volume of the cell wall material (represented as a solid white volume) to the volume enclosing the cell wall. The volumes are binarized by thresholding and the cell wall material is considered by counting the number of white voxels from the binarized images. As thresholding method, we use the region growing algorithm available in the software. The approach to this segmentation algorithm considers an initial "seed point"

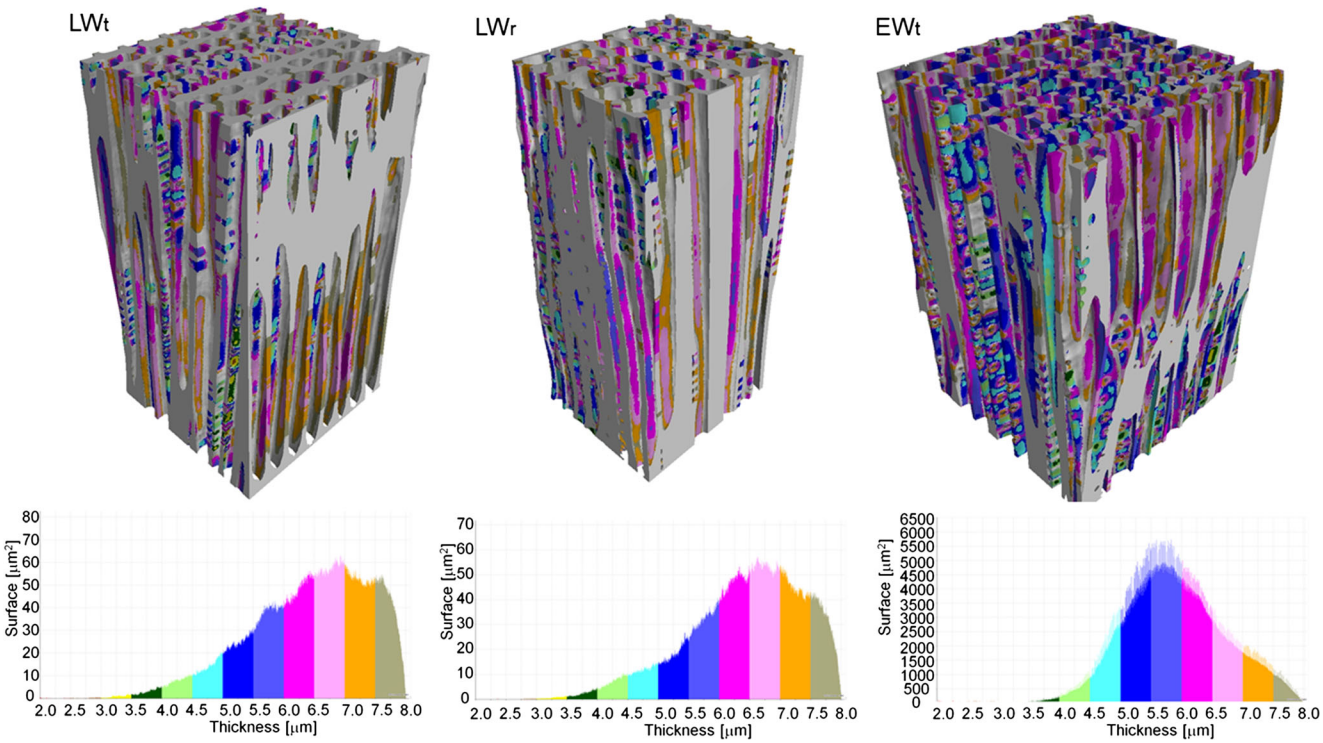

Fig. 9 3D distribution map of the cell wall thickness on the ROI 1 located in the centre of the wood samples considered for this analysis

Table 3 Cell wall thickness, porosity, cells number, tangential/radial swelling and T/R swelling ratio of ROI 1 and ROI 2 shown in Fig. 8, for three samples

	LW_t		LW_r	EW_t	
	ROI 1	ROI 2	ROI 1	ROI 1	ROI 2
Average cell wall thickness [μm]	7.5		6.0	5.7	
Porosity [%]	54		60	65	
Cell number	60	49	46	51	29
Total tangential swelling [%]	2.0	1.0	5.3	2.6	0.3
Total radial swelling [%]	2.5	2.1	1.0	1.1	1.2
T/R swelling ratio	0.8	0.5	5.3	2.4	0.25

which grows incorporating all the voxel neighbours which respect certain criteria of connectivity [22, 23]. In this way, all the voxels which follow similar criteria are added to the initial volume, thus determining the cell wall volume. The samples porosity varies between 54 % in latewood up to 65 % in the earlywood tissue. Such information provides a basic characteristic of each sample.

The wall thickness analysis performed using an existing module in the software allows to first identify cell walls and then measure their thicknesses. We allocate colours per cell wall thickness for illustration in Fig. 9. The histograms of each dataset indicate how the cell wall thickness in latewood is covering a wider range of values than earlywood. The average cell wall thickness for each sample is given in Table 3.

The swelling/shrinkage strains are determined by affine registration as explained in detail in [1]. In general, a 3D affine transformation, f, which maps two volumes by a linear function, is defined by twelve parameters: three for translation, three for rotation, three for scaling and three for shear. Mathematically such mapping can be described as

$$\overline{x}' = f\left(\overline{x}\right) = \overline{\overline{A}}\,\overline{x} + \overline{T} \tag{2}$$

where $\overline{x}'$ is the transformed and $\overline{x}$ the original image coordinates, $\overline{\overline{A}}$ is a 3×3 matrix of real numbers referred to the shear, scale and rotation contribution and $\overline{T}$ is a column translation vector. In practice, the affine deformation hypothesis does not necessarily hold exactly since non-affine deformations can occur. We assume in this paper that the affine deformation is a good approximation for describing the deformation between the two volumes, especially for the ROIs I in the centre of the samples.

We consider the state at 15 % RH as the reference state and we calculate the relative deformation at the states of the other RHs. We split each dataset into 5 stacks of 150 slices each and register each stack, allowing to calculate the average strains in each direction with respective standard deviations.

The results of this calculation are reported in Figs. 10 for ROI1 and Figs. 11 for ROI2. Table 3 includes the total tangential and radial swelling percentage, i.e. considering the reference state at 15 % and the derformed state at 85 %, and the tangential to radial swelling ratios.

The results reported in Table 3 show that the tangential to radial swelling ratios are equal to 0.8 in latewood sample subjected to tangential restraint and 5.3 for the latewood sample restrained radially. In [2], this ratio in homogeneous tissues of similar density is around 1.3. Thus, the device prevents enough tangential swelling to reduce the ratio from

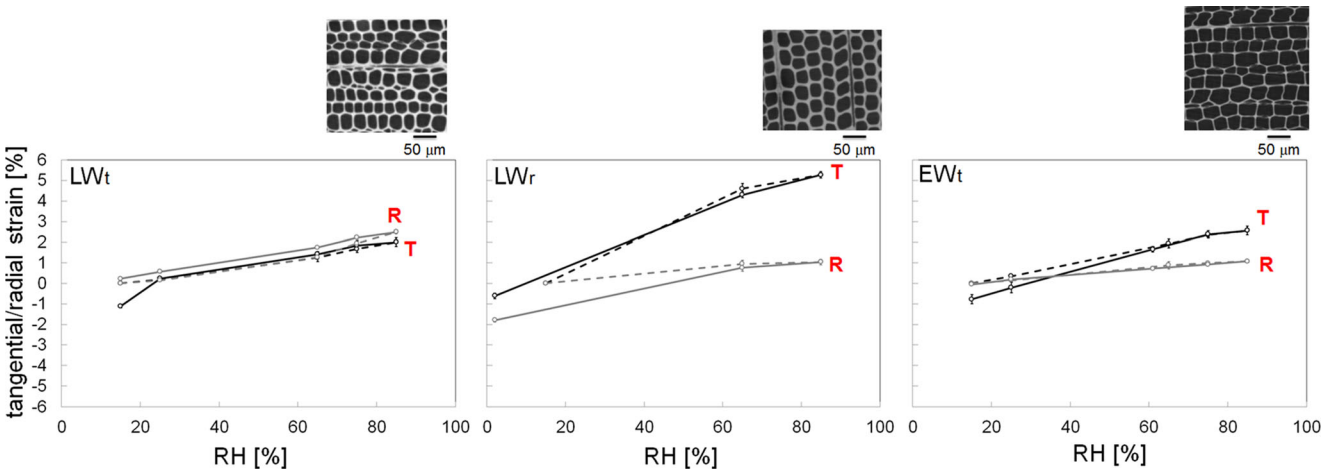

Fig. 10 Tangential strains (*black line*) and radial strains (*grey line*) calculated for ROI 1 in LW_t, LW_r and EW_t. *Continued lines* for desorption conditions and dashed lines for adsorption conditions. The error bars are the standard deviations on each measurement point

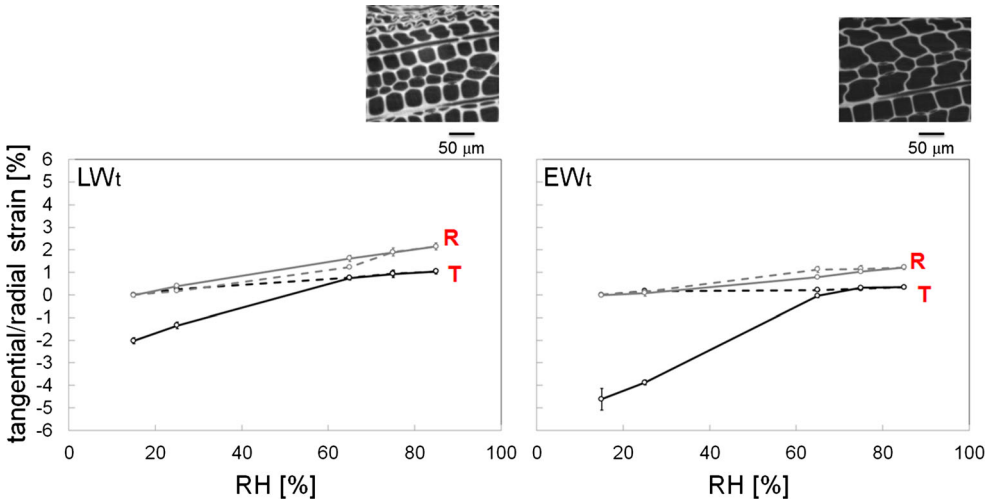

Fig. 11 Tangential strains (*black line*) and radial strains (*grey line*) calculated for ROI 2 in LW_t and EW_t. *Continued lines* for desorption conditions and *dashed lines* for adsorption conditions. The error bars are the standard deviations on each measurement

1.3 to 0.8. However, when the restraint is in the radial direction, the radial swelling is markedly hindered and the ratio augments from 1.3 to 5.3. For the earlywood sample, the restrained swelling led to a ratio of 2.4, which indicate a hindering of tangential swelling when compared to the 3.7 reported in [2].

The ratio seen in the ROI 2 of LW_t is 0.5, which is much lower than the 0.8 seen in centre. The ROI 2 of EW_t, displays a ratio of 0.25, compared to the 2.4 seen in the centre, again showing the larger deformation occurring in earlywood. Thus the extent of deformation is different at the edges of the samples.

To complete the 2D analysis described in the previous section, we performed a three-dimensional affine registration on the four PMMA cubes. Here, we considered the whole stack of 750 images at 15 and 85 % RH and we cut out the regions containing the wood samples in order to align only the cube surfaces. The results are reported in Table 4.

The maximum volumetric swelling of the cubes with less or nor contact with the wood samples (LWr, EWr) is slightly lower compared with the one calculated in the case of a perfect contact (LWt, EWt). However, the volumetric swelling in PMMA is really negligible compared with the swelling in wood due to moisture sorption.

The swelling strains and the anisotropic ratios are clear evidences of the restraining role of the PMMA cubes on the wood samples.

Table 4 Volumetric swelling of the four PMMA cubes under wood swelling pressure and hygroscopic loading

Loading direction	LW_t	LW_r	EW_t	EW_r
Volumetric swelling [%]	0.55	0.35	0.42	0. 32

Conclusions

The three dimensional evidence, combined with the 2D calculation on the slot surface and the sorption analysis highlight the adequacy of the PMMA cube as restraining device.

The cube size was optimized by performing finite element simulations in order to achieve the desired rigidity. The experimental tests performed with the optical microscope,lead to the observation of higher stiffness in the two cubes under swelling load and higher sensitivity to mechanical stress in the $3\times3\times3$ mm^3 cube. These preliminary investigations bring on the conclusion that the optimal size for the PMMA cube to operate as restraining device is of $4\times4\times4$ mm^3. With this device, we were able to obtain a very good contact between PMMA and wood in most of the observed surfaces, leading to the study of the hygro-mechanical properties of wood subjected to restraining conditions.

The strains are strongly dependent on the swelling properties of wood at the different moisture content values. In fact, as latewood swells more than earlywood in tangential and radial directions, the strains in the cubes containing latewood are higher than the strains in cubes with earlywood. These observations are highlighted in 2D by affine registration on the slot surface and in 3D on different regions of interest of the wood samples and on the PMMA cubes. We show that the restraining device successfully prevents the free swelling of wood during moisture adsorption, thus modifying significantly the anisotropy of swelling.

As general conclusion, for future investigations on the mechanical properties of wood with respect to moisture content at cellular scale, the PMMA device shows an adequate level of strain to operate as restraining device. This restraining experiment is also appropriate for a further characterization of the local deformations in the wood cells and of the anisotropy/isotropy in swelling of latewood and earlywood induced by variations in moisture conditions and could provide the

necessary date for a further understanding of the impact of differential swelling at timber scale.

Acknowledgments We greatly acknowledge the team at the TOMCAT beamline Swiss Light Source, Paul Scherrer Institut which has supported the experiments. In particular, Prof. Dr. Marco Stampanoni (ETHZ and PSI) and Dr. Sarah Irvine (PSI).

We would like to acknowledge the Boerlin Company, in Switzerland (http://www.boerlin.ch/) for the fabrication of the PMMA cubes.

We acknowledge the technicians at the Department of Building Science and Technology (EMPA), in particular Stephan Carl for his excellent and important support during the experimental work.

Finally, we acknowledge the Swiss National Science Foundation under grant no. 125184 for the financial support.

References

1. Derome D, Griffa M, Koebel M, Carmeliet J (2011) Hysteretic swelling of wood at cellular scale probed by phase-contrast X-ray tomography. J Struct Biol 173(1):180–190
2. Patera A, Derome D, Griffa M, Carmeliet J (2013) Hysteretic in swelling and in sorption of wood tissues. J Struct Biol. doi:10.1016/j.jsb.2013.03.003
3. Hittmeier ME (1967) Effect of structural direction and initial moisture content on swelling rate of wood. Wood Sci Technol 1(2):109–121
4. Simpson WT, Skaar C (1968) Effect of restrained swelling on wood moisture content. U.S.D.A. Forest Service Research note FPL-0196
5. Narayanamurti D, Mahajan PC (1954) Rheology of wood - part II. The swelling and shrinkage of wood under mechanial restraint. Appl Sci Res 5(6):389–410, ISSN 0003–6994
6. Bolton AJ, Jardine P, Vine MH, Walker JCF (1974) The swelling of wood under mechanical restraint. Holzforschung - Int J Biol Chem Phys Technol Wood 28(4):138–145
7. Moliński W, Roszyk E (2010) Restriction of swelling of wood subjected to bending stress and moistening in the compressed zone. Acta Sci Pol Silv Colendar Rat Ind Lignar 9(1):35–43
8. Schneider P, Leychuk A, Müller R (2010) Automated micro-compression device for dynamic image-guided failure assessment of bone ultrastructure and bone microdamage. XBiomed Tech 55(Suppl 1) 2010 by Walter de Gruyter • Berlin • New York. doi:10.1515/BMT.2010.399
9. Zauner M, Keunecke D, Mokso R, Stampanoni M, Niemz P (2012) Synchrotron-based tomographic microscopy (SbTM) of wood: development of a testing device and observation of plastic deformation of uniaxially compressed Norway spruce samples. Holzforschung 66:973–979. doi:10.1515/hf-2011-0192, Walter de Gruyter • Berlin • Boston
10. Lacroix H, Philips Research Europe (2007) Thermohygroelastic properties of polymethylmethacrylate. Project: Galaxy (2005–054)
11. Shen J, Chen CC, Sauer JA (1985) Effects of sorbed water on properties of low and high molecular weight PMMA: 1. Deformation and fracture behaviour. Polym Pap 26(4):511–518
12. Tobolsky AV, McLoughlin JR (1952) Elasto-viscous properties of polyisobutylene. V. The transition region. J Polym Sci 543–553. doi:10.1002/pol.1952.120080512
13. Ishiyama C, Higo Y (2001) Effect of humidity on Young's modulus in poly(methyl methacrylate). J Polym Sci B Polym Phys 40(5):460–465. doi:10.1002/polb.10107
14. Hubbell JH, Seltzer SM (1995) Tables of X-ray mass attenuation coefficients and mass energy-absorption coefficients from 1 keV to 20 MeV for elements Z = 1 to 92 and 48 additional substances of dosimetric interest. Note on the X-ray attenuation databases, NISTIR 5632
15. Seltzer SM (1989) Electron and positron stopping powers of materials. Database version 2.0, NIST standard reference. Database 7
16. Tynnyi AN, Mikitishin SI, Velikovskii AA, Khomitskii Yu N, Kolevatov Yu A (1967) Effect of X-rays on the strength of polymethylmethacrylate. Soviet Materials Science: a transl of Fiziko-khimicheskaya mekhanika materialov/Academy of Sciences of the Ukrainian SSR 3(1):31–33. doi:10.1007/BF00716639
17. Virta J, Koponen S, Absetz I (2006) Measurement of swelling stresses in spruce (Picea abies) samples. Build Environ 41(8):1014–1018
18. Paganin D, Mayo S, Gureyev T et al (2002) Simultaneous phase and amplitude extraction from a single defocused image of a homogeneous object. J Microsc 206:33–40
19. Marone F, Stampanoni M (2012) Regridding reconstruction algorithm for real-time tomographic imaging. J Synchrotron Radiat 19:1029–1037. doi:10.1107/S0909049512032864
20. Derome D, Rafsanjani A, Patera A, Guyer R, Carmeliet J (2012) Hygromorphic behaviour of cellular material: hysteretic swelling and shrinkage of wood probed by phase contrast X-ray tomography. Philos Mag 92(28–30):2012. doi:10.1080/14786435.2012.715248
21. Pieper S, Halle M, Kikinis R (2004) 3D SLICER. Proceedings of the 1st IEEE International Symposium on Biomedical Imaging: From Nano to Macro 632–635
22. Petrou M, Bosdogianni P (2004) Image processing the fundamentals. Wiley, UK
23. Patera A, De Nunzio G, Tommasi E (2007) Sistemi matematico-fisici per la ricerca di noduli polmonari in immagini CT. Bachelor Thesis, Università del Salento, Italy. http://www.dmf.unisalento.it/~denunzio/allow_listing/TESI/Alessandra_Patera_Tesi.pdf